1999

A Two-Dimensional Analytic Tidal Model for a Narrow Estuary of Arbitrary Lateral Depth Variation: The Intratidal Motion

Chunyan Li
Old Dominion University

Arnoldo Valle-Levinson
Old Dominion University

Original Publication Citation

Li, C. Y., & Valle-Levinson, A. (1999). A two-dimensional analytic tidal model for a narrow estuary of arbitrary lateral depth variation: The intratidal motion. *Journal of Geophysical Research: Oceans, 104*(C10), 23525-23543. doi:10.1029/1999jc900172

JOURNAL OF GEOPHYSICAL RESEARCH, VOL. 104, NO. C10, PAGES 23,525–23,543, OCTOBER 15, 1999

A two-dimensional analytic tidal model for a narrow estuary of arbitrary lateral depth variation: The intratidal motion

Chunyan Li and Arnoldo Valle-Levinson

Center for Coastal Physical Oceanography, Old Dominion University, Norfolk, Virginia

Abstract. An innovative method is introduced to solve a two-dimensional, depth-averaged analytic model for narrow estuaries or tidal channels with arbitrary lateral depth variations. The solution is valid if the lateral variation of the amplitude of tidal elevation ($|\Delta a|$) is small, i.e., $|\Delta a| \ll a$, where a is the amplitude of the tidal elevation. This assumption is supported by a 60-day observation of elevation in the James River Estuary using pressure sensors at both sides of a cross section of the estuary. The error introduced by the solution is of the order of $|\Delta a|/a$, which has a maximum of $\sim$ 5% in the James River Estuary. The propagation of the tidal wave (elevation) is therefore essentially one- dimensional (along the estuary), regardless of the depth distribution, whereas tidal velocity has a strong transverse shear and is three- dimensional in general. Dozens of depth functions in six groups of various forms are used to calculate the solution. The tidal velocity is highly correlated with the bathymetry. The largest amplitude of the along-channel velocity is in the deepest water. The phase of the along-channel velocity in the shallow water leads that in deep water, causing a delay in time of flood or ebb in the deep water. The transverse velocity is generally small in the middle of a channel but reaches its maximum over the edges of bottom slopes. The depth function has a significant effect on the ellipticity and the sense of rotation of the tidal ellipses. By fitting the observed phase of semidiurnal tide in the James River Estuary to the phase of the momentum equation, we have obtained optimal values of the drag coefficient: 1.5×10^{-3} and 1.8×10^{-3} for the spring and neap tides, respectively. Then we apply these values of the drag coefficient and the model to the James River Estuary using the real bathymetry. Results show remarkable agreement between the observations and the model along the transects for both spring and neap tides. The cross-channel phase difference of the along-channel velocity between the channel and the shoal is found to be $\sim$ 1 hour, a value consistent with that from the model. The model-estimated lateral variation of elevation is 2.5% of the tidal amplitude, which is slightly smaller than the observed value.

1. Introduction

Tidal motion in estuaries is induced by tidal waves generated in the ocean and propagated into shallow water. This is often referred to as the "cooscillating tide." One of the most quoted earliest studies on the cooscillating tide was that of *Taylor* [1921]. Taylor's work showed that a cooscillating tide in a semi-enclosed basin with rotation was a superposition of an incident Kelvin wave, a reflected Kelvin wave, and Poincaré waves. If the effect of rotation is small, this cooscillating tide degenerates to simple incident and reflected waves which are applicable to problems of narrow estuaries and tidal rivers [*Lamb*, 1932; *Ippen and Harleman*, 1961; *Officer*, 1976]. Here a "narrow" estuary is one with a width smaller than the barotropic Rossby radius $R = \sqrt{gh}/f$, where g, h, and f are the acceleration due to gravity, the water depth, and the Coriolis parameter, respectively.

The classic tidal wave solutions found in standard textbooks [e.g., *Lamb*, 1932; *Defant*, 1961; *Proudman*, 1953; *Officer*, 1976] are for simple bathymetry configurations, mostly constant depth problems. Tides, however, like many wave phenomena, can be complicated by at least two factors: the nonlinearities and variable water depth. For problems of strong nonlinearities, an analytical study is often too difficult to accomplish regardless of the depth distribution. In a weakly nonlinear problem of cooscillating tide in an estuary, the effect of nonlinearities is of second order while the variable depth can generate a first-order effect. Thus the

Paper number 1999JC900172.
0148-0227/99/1999JC900172$09.00

first-order problem will be linear and usually tractable. However, only a handful of general wave problems with simple bottom topographies have been resolved. These problems are mostly frictionless, vorticity free, and represented by velocity potentials [*Keller*, 1958; *Carrier*, 1966; *Nachbin and Papanicolaou*, 1992]. As shown by several studies [e.g., *LeBlond*, 1978; *Prandle*, 1985; *Speer and Aubrey*, 1985; *Parker*, 1991], tidal wave motion in estuaries is often highly frictional. *Wang and Craig* [1993] used a linear frictional model for the Hey Estuary (maximum width of 4 km) and solved it analytically. The model, however (like other analytic models), assumed that the estuary had rectangular cross-sections, and the transverse momentum was neglected. Consequently, the effect of the transverse depth variation and the transverse structure of the along-estuary flow could not be resolved.

Depth variations across an estuary are found to be crucial in determining the flushing time or residence time [*Li and O'Donnell*, 1997], which is an important indicator of ecological health and self-cleaning capacity of estuaries [*Oliveira and Baptista*, 1996]. An accurate estimate on the flushing time, on the other hand, requires an accurate knowledge of the intratidal flow field with an adequate spatial resolution across the estuary, which often has a significant transverse depth variation. It is therefore of great interest to solve a frictional tidal wave in an estuary of transverse depth variation. *Li* [1996] has presented some analytic solutions of tidal waves in estuaries with variable depth in both horizontal directions, using a perturbation method. The drawback of a perturbation method is the limitation on the degree of the depth variation. The perturbation solution may not be convergent if the maximum depth difference within the estuary is comparable to or greater than the mean depth.

In this paper, we present a theory for cooscillating tidal motion in tidal rivers and shallow estuaries with arbitrary lateral depth variations, without using a perturbation method. A simplification is made from the fact that the tidal elevation across a narrow estuary has a difference that is much smaller than the amplitude of the elevation, or the elevation is almost laterally uniform. This assumption is verified by examining the lateral derivative of the surface elevation obtained from the momentum balance. In section 2, we present the analytic solution. In section 3, we calculate the solution for dozens of depth profiles and discuss the solution regarding the effect of bathymetry on the strength of flow, tidal ellipses, transverse variation of elevation, and vorticity. We then estimate the error of approximation and the transverse gradient of the surface elevation. In section 4, we discuss the propagation of the wave and compare the results with some observations using a shipborne acoustic Doppler current profiler (ADCP) in the James River Estuary. In section 5, we summarize the results.

2. Formulation

We use a model geometry similar to that of *Li and O'Donnell* [1997]: The model is straight and has parallel side boundaries. However, here we allow an arbitrary lateral depth variation. The x axis is taken to lie along the boundary and points toward the head of the estuary. The y axis lies along the open boundary at $x = 0$. A single-frequency, semidiurnal tide is imposed at the mouth of the estuary. Both the amplitude and the phase of sea level variation at the mouth are assumed to be uniform across the estuary and are specified.

We use the depth-averaged, shallow water momentum and continuity equations [*Li and O'Donnell, 1997*]:

$$\begin{aligned}
&\frac{\partial u}{\partial t} + u\frac{\partial u}{\partial x} + v\frac{\partial u}{\partial y} - fv = -g\frac{\partial \zeta}{\partial x} - \beta\frac{u}{h} + \frac{\beta}{h^2}u\zeta \\
&\frac{\partial v}{\partial t} + u\frac{\partial v}{\partial x} + v\frac{\partial v}{\partial y} + fu = -g\frac{\partial \zeta}{\partial y} - \beta\frac{v}{h} + \frac{\beta}{h^2}v\zeta \\
&\frac{\partial \zeta}{\partial t} + \frac{\partial (h+\zeta)u}{\partial x} + \frac{\partial (h+\zeta)v}{\partial y} = 0
\end{aligned} \tag{1}$$

where $u, v, \zeta, h, x, y, t, \beta, f$, and g are longitudinal velocity, lateral velocity, elevation, water depth, longitudinal coordinate, lateral coordinate, time, friction coefficient, Coriolis parameter, and the gravitational acceleration, respectively. The friction coefficient β is defined by [*Proudman*, 1953; *Parker*, 1984]

$$\beta = \frac{8C_D U_0}{3\pi} \tag{2}$$

where C_D and U_0 are the bottom drag coefficient and the magnitude of the longitudinal velocity, respectively. The friction coefficient β, which may be a function of y, is dependent on the velocity amplitude and the drag coefficient. It will be shown later in this section that the solution allows the drag coefficient C_D to be any reasonable function of y. In our study, we will use a constant C_D for simplicity. *Li* [1996] has discussed in depth the effect of a variable friction coefficient β on tidal and subtidal flows. The results showed no fundamental differences.

It can be shown, by a scaling analysis, that the advection terms, the cross-product frictional terms (i.e., $\beta u\zeta/h^2$ and $\beta v\zeta/h^2$), and the Coriolis force term in the along-channel momentum have higher orders of magnitudes (than other terms) [e.g., *Li*, 1996]. The Coriolis force in the transverse momentum, on the other hand, can be more important than the local acceleration ($\partial v/\partial t$). This is because a typical estuary has a length (L) much larger than its width (D), which leads to the scaling $fU_0/\sigma V_0 \sim fL/\sigma D$ (the ratio between the Coriolis force and transverse local acceleration) $\gg 1$, where U_0 and V_0 are the longitudinal and transverse velocity scales, respectively, and σ is the angular frequency of the tide. We will therefore keep the Coriolis force in the transverse momentum. To keep the gener-

ality of the solution, we will also keep the local acceleration $\partial v/\partial t$. The linearized equations are then

$$\begin{aligned} \frac{\partial u}{\partial t} &= -g\frac{\partial \zeta}{\partial x} - \frac{\beta}{h}u \\ \frac{\partial v}{\partial t} + fu &= -g\frac{\partial \zeta}{\partial y} - \frac{\beta}{h}v \\ \frac{\partial \zeta}{\partial t} + h\frac{\partial u}{\partial x} + \frac{\partial hv}{\partial y} &= 0 \end{aligned} \tag{3}$$

The depth is assumed to be a sufficiently smooth (differentiable) but otherwise arbitrary function of the across-estuary position:

$$h = h(y) \tag{4}$$

For a single-frequency cooscillating tide, the solution can be expressed as

$$u = Ue^{i\sigma t}, \qquad v = Ve^{i\sigma t}, \qquad \zeta = Ae^{i\sigma t} \tag{5}$$

where σ, i, U, V, and A are the angular frequency of the tide, the unit imaginary number $\sqrt{-1}$, the complex amplitude of the longitudinal velocity, the complex amplitude of the lateral velocity, and the complex amplitude of the tidal elevation, respectively.

Substituting (5) into (3) yields

$$\begin{aligned} i\sigma U &= -g\frac{\partial A}{\partial x} - \frac{\beta}{h}U \\ i\sigma V + fU &= -g\frac{\partial A}{\partial y} - \frac{\beta}{h}V \\ i\sigma A + h\frac{\partial U}{\partial x} + \frac{\partial hV}{\partial y} &= 0 \end{aligned} \tag{6}$$

In the following, we use the first and third equations of (6), i.e., the x- momentum and the continuity, respectively, to solve for U and A. The y- momentum equation will not need to be referred to again until we solve for $\partial A/\partial y$ to verify the assumption that $\partial A/\partial y$ is small. For a cooscillating tide problem, the tidal amplitude at the mouth is usually known. The longitudinal velocity at the head ($x = L$, a solid boundary) vanishes. Since the side boundaries are parallel to each other and the y axis is perpendicular to the side boundaries, the lateral velocity at the side boundaries ($y = 0, D$) must be zero. Therefore the boundary conditions associated with (6) are

$$A\Big|_{x=0} = a, \qquad \frac{\partial A}{\partial x}\Big|_{x=L} = 0, \qquad V|_{y=0,D} = 0 \tag{7}$$

The first equation of (6) yields

$$U = -\frac{g}{i\sigma + \beta/h}\frac{\partial A}{\partial x} \tag{8}$$

$$\frac{\partial U}{\partial x} = -\frac{g}{i\sigma + \beta/h}\frac{\partial^2 A}{\partial x^2} \tag{9}$$

In a study by *Friedrichs and Hamrick* [1996], a similar dynamical balance was used in which the pressure gradient ($\partial A/\partial x$) was assumed known and independent of y. *Li* [1996] has shown that on the basis of a perturbation solution, the lateral variation of tidal elevation in an estuary or tidal river of a few kilometers wide is very small compared to that of the longitudinal variation. We therefore assume that the lateral variation of elevation is negligible in the x- momentum and the continuity equations. The complex amplitude of the tidal elevation is thus taken to be approximately independent of y, which leads to a dramatic simplification of the solution. The validity of this approximation will be verified in section 3. It will also be shown in section 3.5 that the transverse gradient of the elevation $|\partial A/\partial y|$, obtained from the y- momentum (second equation of (6)), is indeed very small in the present problem of interest. Note that similar approximations, which are justified by scaling arguments, have been used by *Li* [1996] and *Li and O'Donnell* [1997] in the study of tidally induced residual circulation. These studies produced results that are almost identical to those from exact solutions [*Li*, 1996].

The differences between the work of *Friedrichs and Hamrick* [1996] and the present work are that (1) the former used a prescribed value for $\partial\zeta/\partial x$, whereas the present work solves the problem in the context of a cooscillating tidal wave, in which the pressure gradient is given by the solution, and (2) the former solved the velocity field $u(y, z)$ at one cross section in which z is the vertical coordinate, whereas the present work solves both the tidal elevation and the depth-averaged tidal velocity throughout the model domain. Note that by assuming a known pressure gradient at a single position, the solution of *Friedrichs and Hamrick* was only valid at that position and could not demonstrate the characteristics of a tidal wave (with incident and reflected wave components), since the tidal elevation was not solved, while here our objective is to solve the tidal wave problem.

In order to solve for A from the third equation of (6), we multiply (9) by h and then integrate the product across the estuary from $y = 0$ to $y = D$, which yields

$$\int_0^D h\frac{\partial U}{\partial x}dy = -\int_0^D \frac{gh}{i\sigma + \beta/h}\frac{\partial^2 A}{\partial x^2}dy \approx \mathcal{F}\frac{\partial^2 A}{\partial x^2} \tag{10}$$

where

$$\mathcal{F} = -\int_0^D \frac{gh}{i\sigma + \beta/h}dy \tag{11}$$

Note that we have neglected the lateral variation of $\partial^2 A/\partial x^2$ in obtaining (10). The error of the approximation of (10) is $\mathcal{F}\partial^2|\Delta A|/\partial x^2$, where ΔA is the magnitude of the lateral variation of A. The relative error is therefore $|\partial^2 \Delta A/\partial x^2|/|\partial^2 A/\partial x^2| \sim |\Delta A|/|A|$, or the lateral variation of A over the amplitude of A. Integrating the third equation of (6) across the estuary yields

$$i\sigma AD + \mathcal{F}\frac{\partial^2 A}{\partial x^2} = 0 \tag{12}$$

Again, we have used the assumption that A is laterally independent in obtaining (12). We have also applied (10) and the boundary condition for V in (7). Equation (12) has a solution satisfying the boundary conditions (7) for A:

$$A = a\frac{\cos[\omega(x-L)]}{cos(\omega L)} \tag{13}$$

in which

$$\omega^2 = \frac{i\sigma D}{\mathcal{F}} \tag{14}$$

Consequently, we have, by virtue of (8), (9), and (13) the solutions for U and the along-channel gradients of A and U:

$$U = \frac{g}{i\sigma + \beta/h}\frac{a\omega}{\cos(\omega L)}\sin[\omega(x-L)] \tag{15}$$

$$\frac{dA}{dx} = -\frac{a\omega}{\cos(\omega L)}\sin[\omega(x-L)] \tag{16}$$

$$\frac{\partial U}{\partial x} = \frac{g}{i\sigma + \beta/h}\frac{a\omega^2}{\cos(\omega L)}\cos[\omega(x-L)] = \frac{g\omega^2}{i\sigma + \beta/h}A \tag{17}$$

Note that if either the depth function is dependent on x or the width D varies along the channel, the coefficients of (12) will no longer be constant. For variable coefficients, a general explicit solution for (12) is not readily obtainable. For a constant depth (h=const) and exponential width, an analytic solution can be derived, but it can not be extended to the case when the depth is variable. With a lengthy but straightforward derivation, A, U, and their derivatives can be expressed in terms of their real and imaginary parts (see appendix). Evidently, the lateral dependence of U is dictated by the form of $h(y)$ as shown in (15). For a constant h, the solution is the same as that of previous theories [e.g., *Ippen and Harleman*, 1961; *Officer*, 1976]. Substituting (17) into the third equation of (6) yields

$$i\sigma A + \frac{gh\omega^2}{i\sigma + \beta/h}A + \frac{\partial hV}{\partial y} = 0 \tag{18}$$

which can be used to solve V by integration with respect to y:

$$V = -\frac{1}{h}\left(i\sigma y + \int_0^y \frac{gh\omega^2}{i\sigma + \beta/h}dy\right)A \tag{19}$$

It can be shown that for a constant h, V is identically zero. It follows from the second equation of (6) and (19) that

$$\begin{aligned}\frac{\partial A}{\partial y} &= -\frac{1}{g}\left[(i\sigma + \beta/h)V + fU\right] \\ &= \frac{i\sigma + \beta/h}{gh}\left(i\sigma y + \omega^2\int_0^y \frac{gh}{i\sigma + \beta/h}dy\right)A \\ &+ \frac{f}{i\sigma + \beta/h}\frac{\partial A}{\partial x}\end{aligned} \tag{20}$$

from which the magnitude of $\partial A/\partial y$ can be calculated and used to check the assumption that A is almost laterally uniform. The solutions for A, U, and V, i.e., equations (13), (15), and (19), are obtained regardless of the actual form of $\beta(y)$ and therefore allow a variable C_D across the estuary. Physical insights can be obtained from the solution. For instance, from (15), the amplitude of the along-channel velocity is $|U| = \alpha h/\sqrt{\sigma^2 h^2 + \beta^2}$, where α is a constant with a unit of ms^{-2} at a given x. It can be shown that for typical shallow estuaries, the larger h is, the larger $|U|$ will be, although the relationship is not linear, particularly at large h (> 20 m). The dependence of phase of along-channel velocity on the variation of water depth can be seen from the function $-\tan^{-1}(\sigma h/\beta)$, which gives a larger value for a smaller h indicating that both flood and ebb occur first at shallow water. Note that friction (β) is crucial in determining these characteristics of tide: if β is zero, then both $|U|$ and the phase of U will be independent of h. In section 3, we will present some examples for the solution obtained here. We will also estimate the error of the approximation.

3. Results

In this section, different depth functions are applied to the solution obtained in section 2. The depth functions are described first, followed by a discussion of the solution. Emphasis will be given to the effect of the bathymetry. We will examine the strength of the flow, the tidal ellipses, the lateral variation of elevation, and the vorticity, in relation to the depth distribution.

3.1. Depth Functions

For convenience, we present the depth functions in six groups. These functions are chosen as examples to study the effect of arbitrary transverse depth variations with the emphasis on the effect of channel-shoal configuration and bottom slopes. The width D is chosen to be 2000 m for all six groups of depth functions. The first group defines symmetric depth profiles (Figure 1a) represented by the following equation:

$$h(y) = 5 + 3e^{-(y-D/2)^2/b^2} \tag{21}$$

in which y, D, and b are the transverse coordinate, the estuary width, and a parameter that adjusts the depth profile, respectively. This function defines a depth profile with minimum and maximum depth values of 5 and 8 m, respectively. The value of b is between 100 and 1000 m. For $b = 100$ m, (21) represents a flat shoal at each side with a relatively deep funnel-shaped channel in the middle (the uppermost curve in Figure 1a). For $b = 1000$ m, (21) represents a simple v-shaped profile with no flat shoals (the lowest curve of Figure 1a). The second group of depth functions is

$$h(y) = 5 + 3e^{-(y-D/5)^2/150^2} + 3e^{-(y-4D/5)^2/b^2} \tag{22}$$

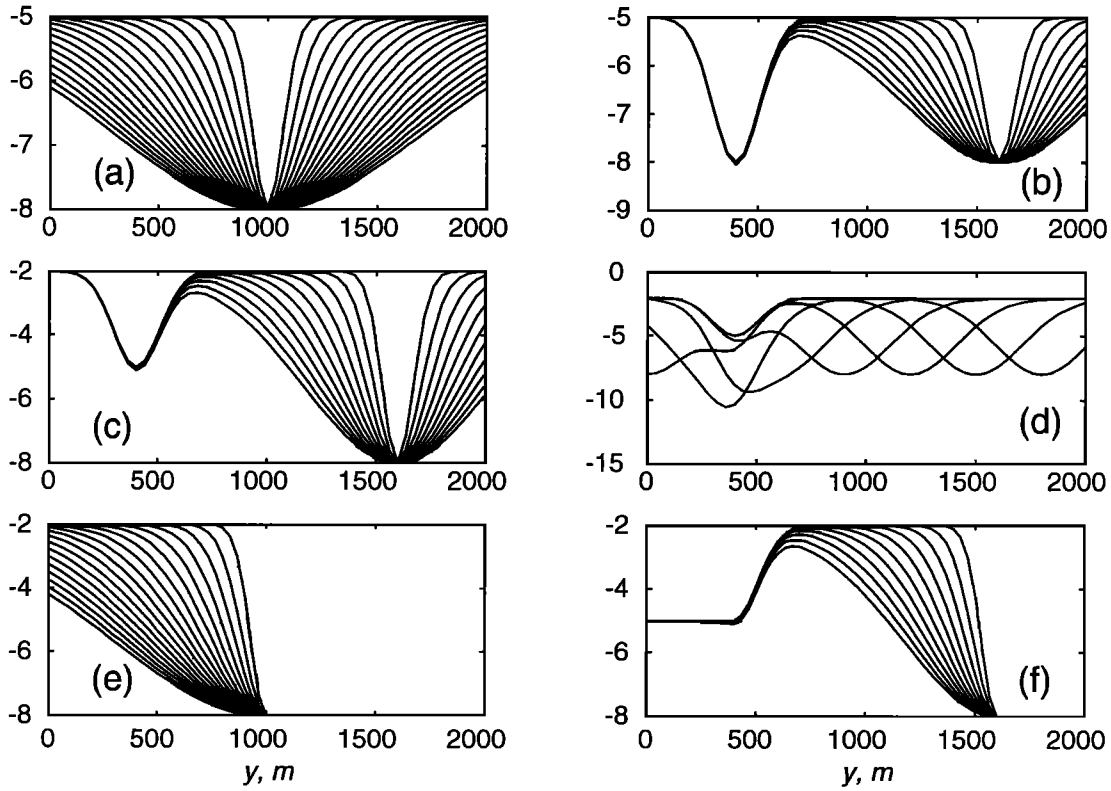

Figure 1. (a–f) Depth (in meters) as a function of transverse distance y. Figures 1a–1f correspond to the depth functions defined in equations (21)–(26), respectively, with given parameter ranges as described in the text.

which represents two separate channels of 8 m deep and a middle shoal with a minimum depth of 5 m (Figure 1b). The value of b is chosen to vary from 100 to 600 m. The third group of depth functions defines two channels of different depths (8 and 5 m, respectively) separated by a shoal of 2 m (Figure 1c), which is expressed as

$$h(y) = 2 + 3e^{-(y-D/5)^2/b^2} + 6e^{-(y-4D/5)^2/b^2} \quad (23)$$

with b varying from 100 to 600 m. The fourth group is defined by

$$h(y) = 2 + 3e^{-(y-D/5)^2/150^2} + 6e^{-(y-y_0)^2/300^2} \quad (24)$$

with y_0 varying from 0 to $0.95D$ (Figure 1d). The variable y_0 results in a channel with variable axial position across the width. Therefore, for those values of y_0 that are away from $D/5$, this depth function produces two channels. As y_0 becomes closer to $D/5$, the two channels tend to merge into one channel. The fifth group defines depth profiles with a flat channel on one side

$$h(y) = \begin{cases} 2 + 6e^{-(y-D/2)^2/b^2} & (y \le D/2) \\ 8 & (y > D/2) \end{cases} \quad (25)$$

Depending on the value of b, which we choose to vary from 100 to 1000 m, the depth defined by (25) decreases either gradually or abruptly from a flat channel to a flat shoal (Figure 1e). The sixth group defines two flat channels with different depths on the two sides, which are separated by a shallow shoal with a minimum depth of 2–3 m in between (Figure 1f). The analytic function of this group is

$$h(y) = \begin{cases} 5 + 6e^{-(y-4D/5)^2/b^2} & (y \le 4D/5) \\ 2 + 3e^{-(y-D/5)^2/150^2} + 6e^{-(y-4D/5)^2/b^2} & (D/5 < y \le 4D/5) \\ 8 & (y > 4D/5) \end{cases} \quad (26)$$

in which b varies from 100 to 600 m. These depth functions are chosen to represent various channel-shoal configurations found in estuaries, and they allow very steep depth profiles that may cause some numerical models to fail.

3.2. Strength of Flow

By applying the depth functions defined in section 3.1, we have calculated the solution. Tidal amplitude at the mouth is chosen to be 1 m for all the calculations. Figures 2–5 show the amplitude of u and the amplitude of v with the depth functions defined by (21)–

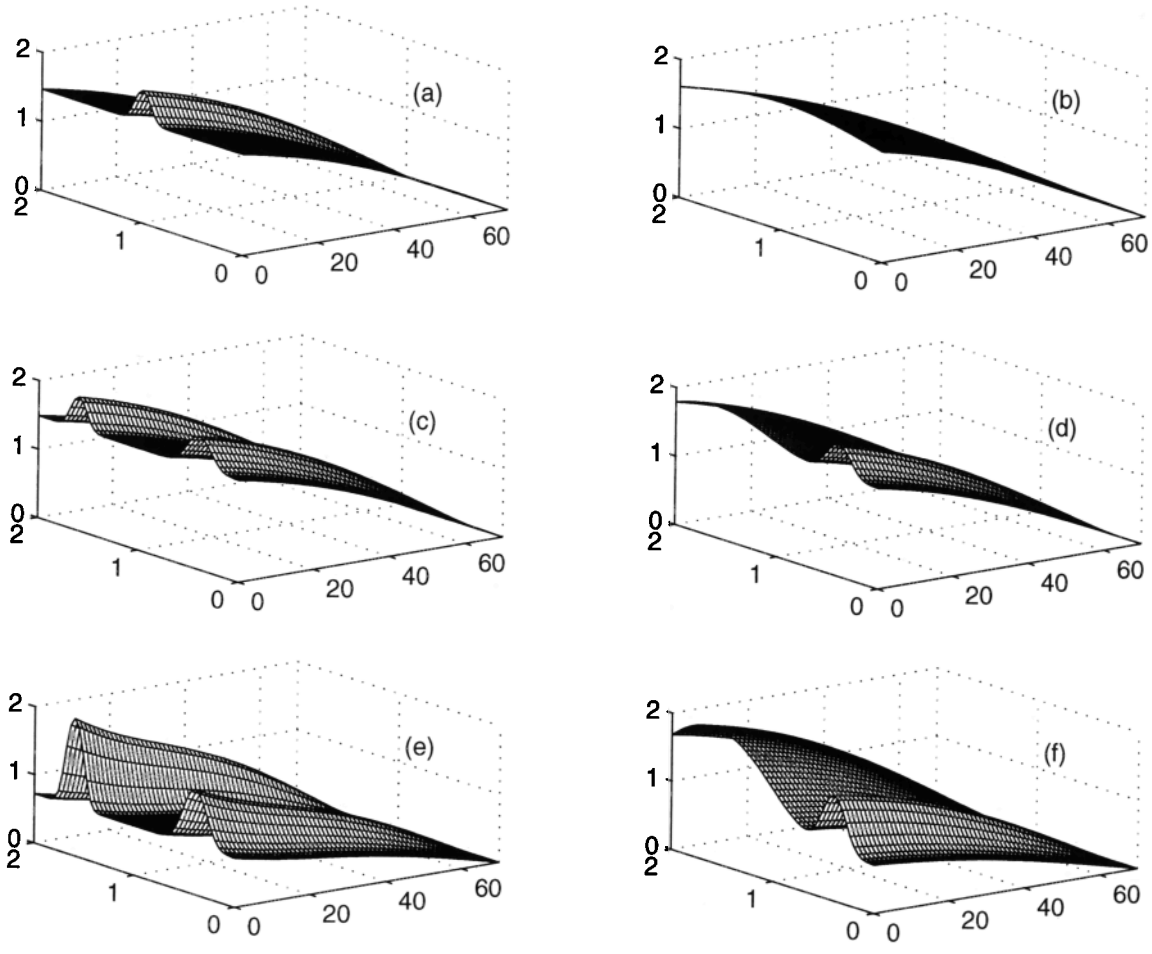

Figure 2. The distribution of the amplitude of longitudinal velocity (m/s) within the model of 2 km wide and 70 km long. (a, b) Distributions corresponding to depth functions defined in Figure 1a with b = 100 and 1000 m, respectively; (c, d) distributions corresponding to depth functions defined in Figure 1b with b = 100 and 600 m, respectively; and (e, f) distributions corresponding to depth functions defined in Figure 1c with b = 100 and 600 m, respectively.

(26). Depth functions corresponding to Figures 2–5 are those of the uppermost and lowermost curves of Figures 1a–1f (i.e., either maximum or minimum values of b or y_0 for the depth functions are selected). A distinct feature of the flow is that the longitudinal velocity u has a larger amplitude in deeper water than it does in shallower water, and it decreases from the mouth to the head. The amplitude of u is also strongly influenced by the rate of change of depth across the channel. The steeper the channel is, the larger the maximum value of the amplitude of u and its lateral shear will be (compare Figure 2a with Figure 2b, Figure 2c with Figure 2d, and Figure 2e with Figure 2f). The lateral distribution of the amplitude of u closely follows the depth function. This can be better presented with a cross-channel view of the amplitude of u at the mouth for all the depth functions (Figures 6a–6f). Obviously, the magnitude of the longitudinal velocity follows the depth function. The number of maxima of the longitudinal flow equals the number of depth maxima.

The amplitude of the transverse velocity component has a different response to the bathymetry. Figures 4 and 5 show the amplitude of v with the same depth functions as those of Figures 2 and 3. For better visualization, Figures 6g–6l show the amplitude of v at the mouth for all the depth functions, just as in Figures 6a–6f. From Figures 4, 5, and 6g–6l, we see that the transverse velocity is zero at the lateral boundaries, an expected result. In addition, it is zero or small (depending on whether the depth is symmetric) in the middle of the channel, and its maximum occurs at the edge of the slopes, i.e., over the shoulder of the channels. The variation of transverse velocity at the edges of slopes may imply a tendency to cause intratidal convergence or divergence at these locations.

3.3. Tidal Ellipses

The discussion in section 3.2 of the flow strength only deals with the amplitude of tidal velocity. The distri-

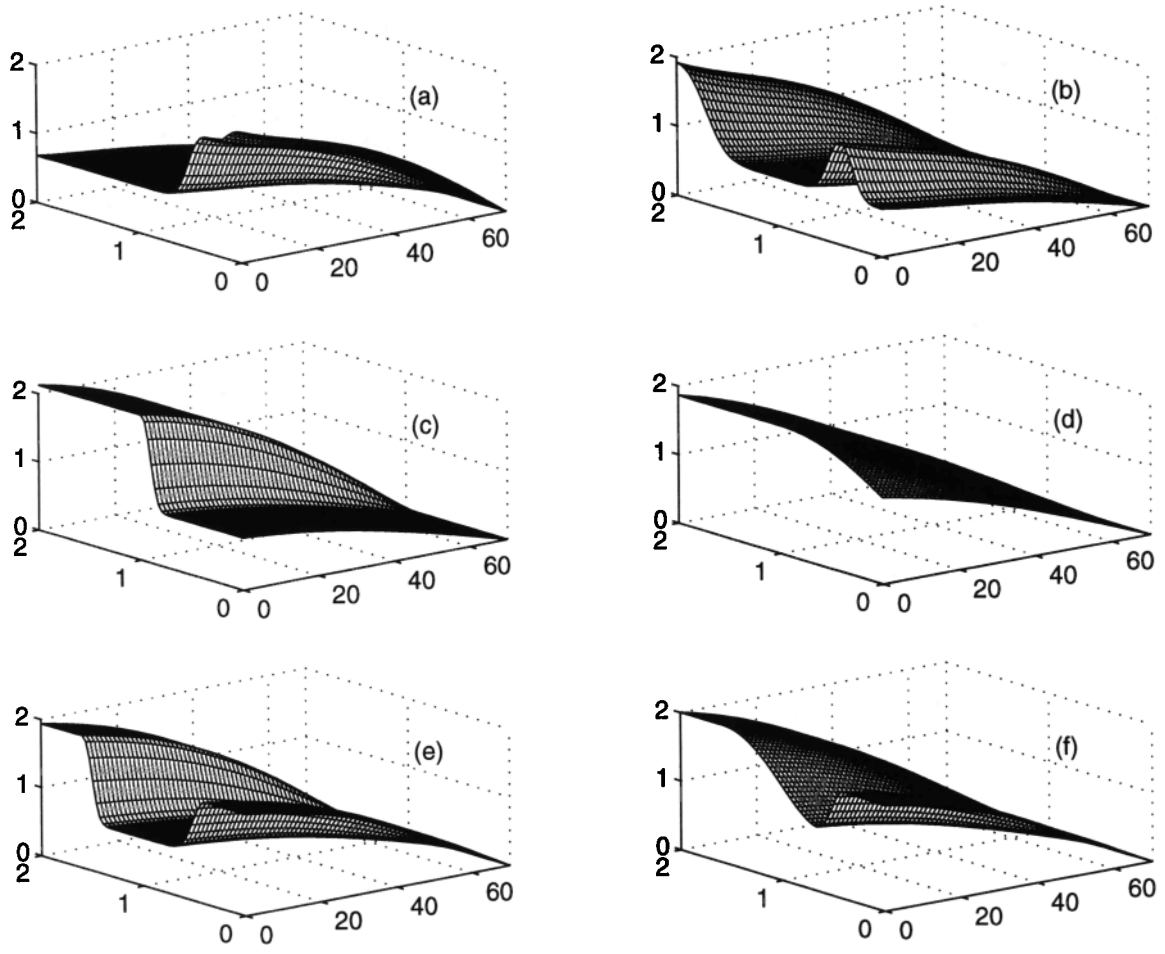

Figure 3. The distribution of the amplitude of longitudinal velocity (m/s) within the model of 2 km wide and 70 km long. (a, b) Distributions corresponding to depth functions defined in Figure 1d with $y_0 = 0$ and $0.95D$, respectively; (c, d) distributions corresponding to depth functions defined in Figure 1e with $b = 100$ and 1000 m, respectively; and (e, f) distributions corresponding to depth functions defined in Figure 1f with $b = 100$ and 600 m, respectively.

bution of the phase of the velocity provides information about the evolution of tidal velocity vectors in a tidal cycle or the orientation, direction of rotation, and the ellipticity of the tidal ellipses. Calculations show that for all the depth functions considered, the phase of the longitudinal flow in deep water always lags that on the shoals as predicted at the end of section 2 by a direct analysis to the solution. Depending on the actual depth function, the phase lag can reach 20°–30° (or 40–60 min) for a semidiurnal tide, comparable to previous observations [*Valle-Levinson and Lwiza*, 1995, 1997]. The distributions of phase and phase differences among ζ, u, and v determine the two-dimensional (2-D) structures of the tidal motion and flow characteristics. In this section, we discuss the tidal ellipses. We show schematically the sense of rotation and ellipticity of the ellipses and the flow vectors at high tides for the depth functions of (21)–(26) with maximum and minimum parameters of selection.

For a better visualization, the transverse velocity has been exaggerated. For depth functions symmetric about a longitudinal axis (Figure 1a), the tidal ellipses are also symmetric about the axis (Figures 7a and 7b). For all depth functions used, there are some common characteristics of the tidal ellipses. First, the tidal ellipses are sensitive to the distribution of depth (Figures 7 and 8). For instance, when b changes from 100 to 600 m in (22), the sense of rotation of the tidal ellipses changes (compare Figure 7c with Figure 7d), indicating that the depth variation has a strong influence on phases. Similar results are obvious by comparing Figure 7e with Figure 7f, Figure 8a with Figure 8b, Figure 8c with Figure 8d, and Figure 8e with Figure 8f. Second, a larger slope of the bottom causes a larger variation in the ellipticity and the magnitude of flow across the slope (compare Figure 7e with Figure 7f, Figure 8c with Figure 8d, and Figure 8e with Figure 8f). Third, the flow is close to a progressive wave at the mouth but

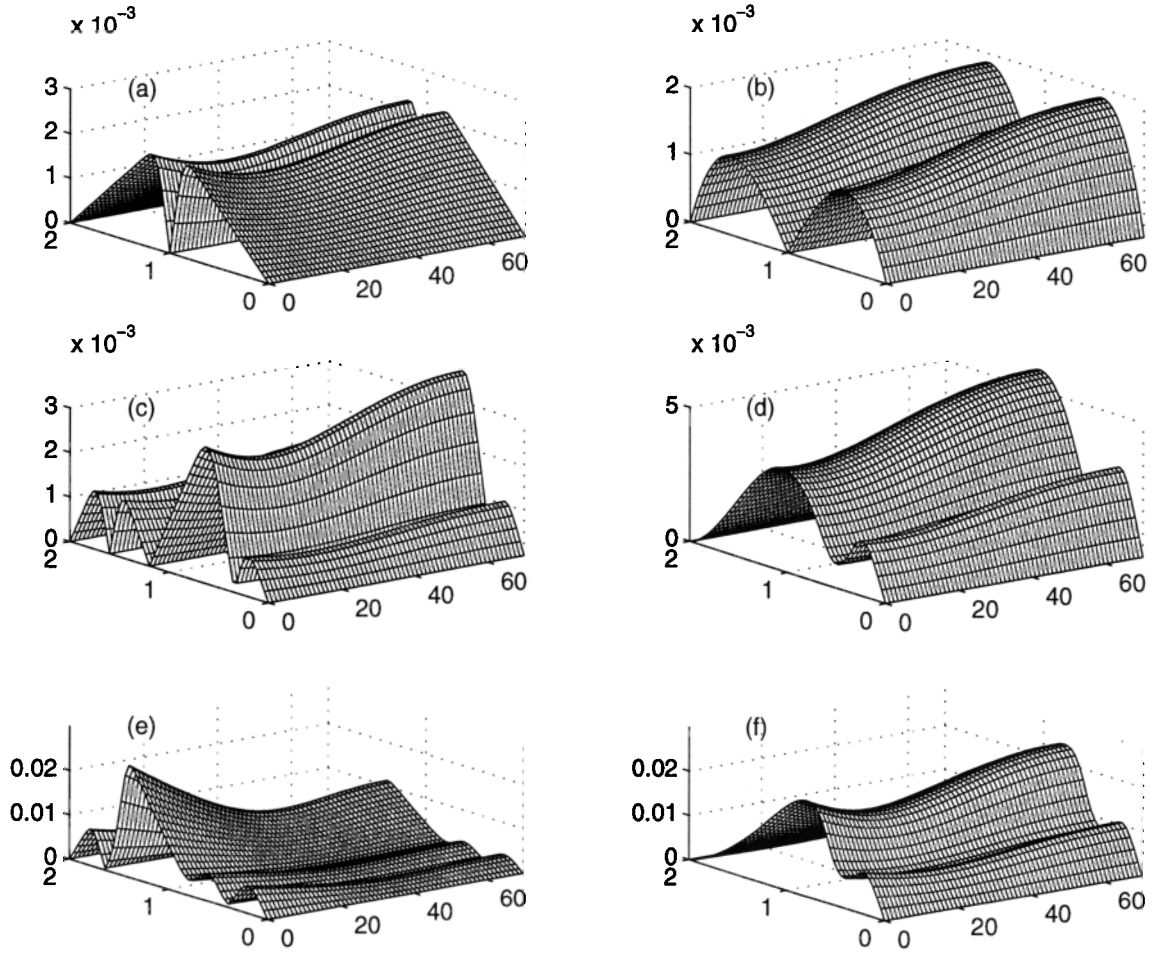

Figure 4. The distribution of the amplitude of transverse velocity (m/s) within the model of 2 km wide and 70 km long. (a, b) Distributions corresponding to depth functions defined in Figure 1a with b = 100 and 1000 m, respectively; (c, d) distributions corresponding to depth functions defined in Figure 1b with b = 100 and 600 m, respectively; and (e, f) distributions corresponding to depth functions defined in Figure 1c with b = 100 and 600 m, respectively.

a standing wave at the head. This can be seen by the position of the circles on the ellipses: at the mouth, the flow at high tide is landward and close to the maximum strength, while in the interior, particularly close to the head, the flow at high tide is close to its minimum strength (Figures 7 and 8). Fourth, when there is a large lateral depth variation with a relatively deep channel and a shallow shoal, there is a significant lateral variation of phase of the velocity, and the flow over shallow water reaches its maximum much earlier than that over deep water does. This can be seen by the circles on the ellipses over shallow water (Figures 7e–8f). This phenomenon has been observed at the Chesapeake Bay Mouth and attributed to the effect of bottom friction [*Valle-Levinson and Lwiza*, 1995]. Fifth, the strongest cross-isobath flow occurs over the largest slopes (Figures 7e, 8a, 8b, 8c, and 8e).

3.4. Vorticity

Because of strong bottom frictions in shallow estuaries, velocity potentials can not be used to formulate the governing equations since vorticity is expected to be important. In the present model, the longitudinal tidal velocity dominates over the transverse velocity as in most narrow estuaries. Therefore the vorticity approximately reflects the transverse shear of the longitudinal velocity. Again, we only show the vorticity distribution for the depth functions with the steepest bottom slopes of (21)–(26) (Figures 9a–9f). In general, the vorticity is larger at the mouth and decreases to zero at the head. The maximum magnitude of the vorticity is 10^{-4} s^{-1} except for the steepest bottom slopes where it can reach 10^{-3}–10^{-2} s^{-1} locally (Figure 9). For the symmetric depth function (21), the vorticity is zero along

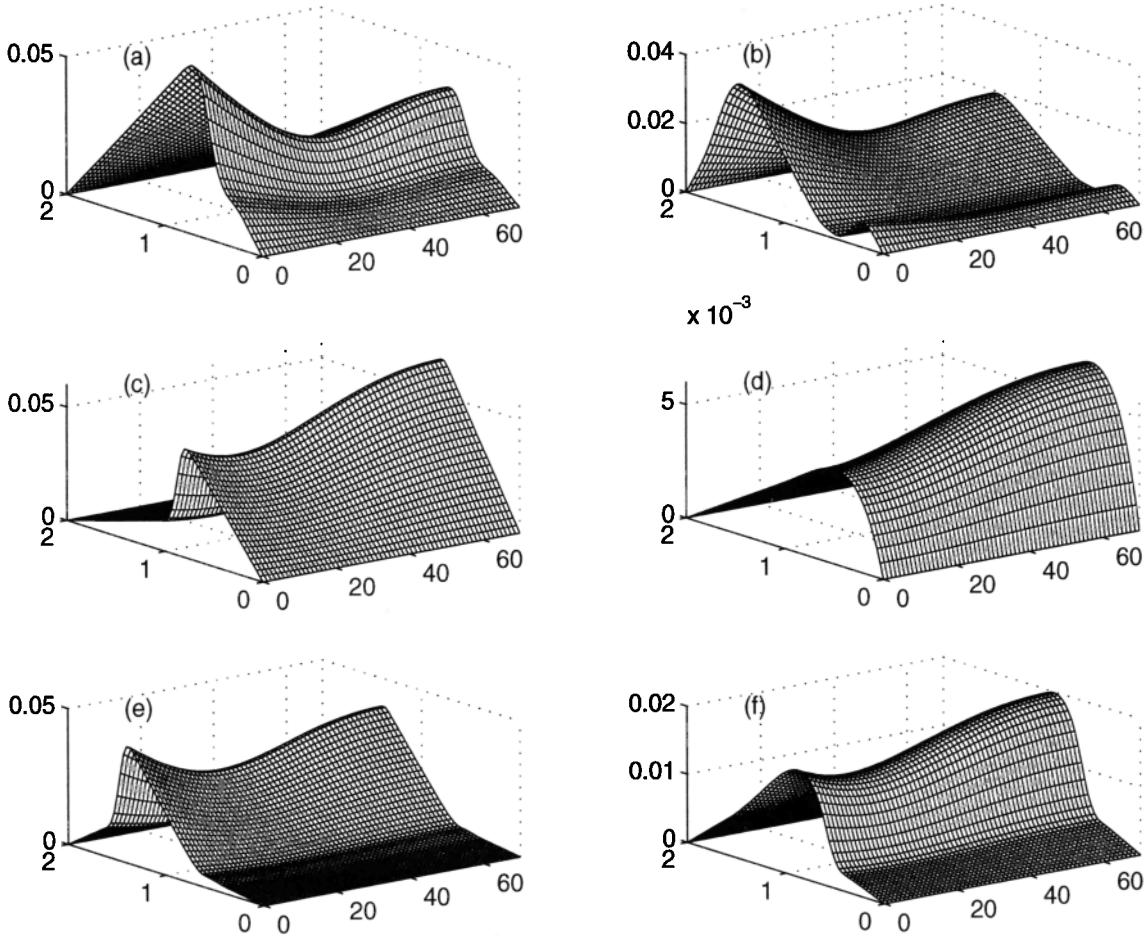

Figure 5. The distribution of the amplitude of transverse velocity (m/s) within the model of 2 km wide and 70 km long. (a, b) Distributions corresponding to depth functions defined in Figure 1d with $y_0 = 0$ and $0.95D$, respectively; (c, d) distributions corresponding to depth functions defined in Figure 1e with $b = 100$ and 1000 m, respectively; and (e, f) distributions corresponding to depth functions defined in Figure 1f with $b = 100$ and 600 m, respectively.

the axis (Figure 9a) with the maximum values on the edges of the bottom slope and close to zero elsewhere in the flat region. Similarly, the magnitude of the vorticity over nonsymmetric bathymetry (Figures 9b–9f) is zero or close to zero in the deep channel and reaches its maximum at the edges of the bottom slopes. Like the other properties of the solution, vorticity is highly affected by the bathymetry. The largest transverse shear of along-channel velocity occurs at the edges of large transverse slopes of the bottom, producing the largest vorticity locally. For gentler depth variations, the vorticity can be smaller than 10^{-4} s^{-1} (not included in Figure 9) and spread across the width rather than being confined to the region of large bottom slopes.

3.5. Error Estimates for the Model

In order to find the solution, we have assumed that the lateral variation of the elevation is small. This approximation introduces an error into the continuity which is used to solve the elevation. Therefore the elevation and thus the velocity (which is obtained in terms of elevation) all have the same order of dynamical error. Since the lateral variation of elevation is of the order of $(\partial\zeta/\partial y)D$, we can define the ratio between this quantity and the amplitude of the elevation as the relative error as discussed in section 2. Figures 10a–10f show the relative error of the solution with the depth functions defined in (21)–(26), which is of the order of 5×10^{-2}, or 5%. With a 1 m tidal amplitude, a 5% error is equivalent to a lateral difference of elevation of 5 cm, a small value compared to the tidal amplitude.

For wide estuaries, for instance $D \sim 20$ km, the lateral variation of elevation can be larger not only because of the effect of the bathymetry but also because of a more likely nonuniform forcing across the width at the mouth. In addition, Coriolis force will become more im-

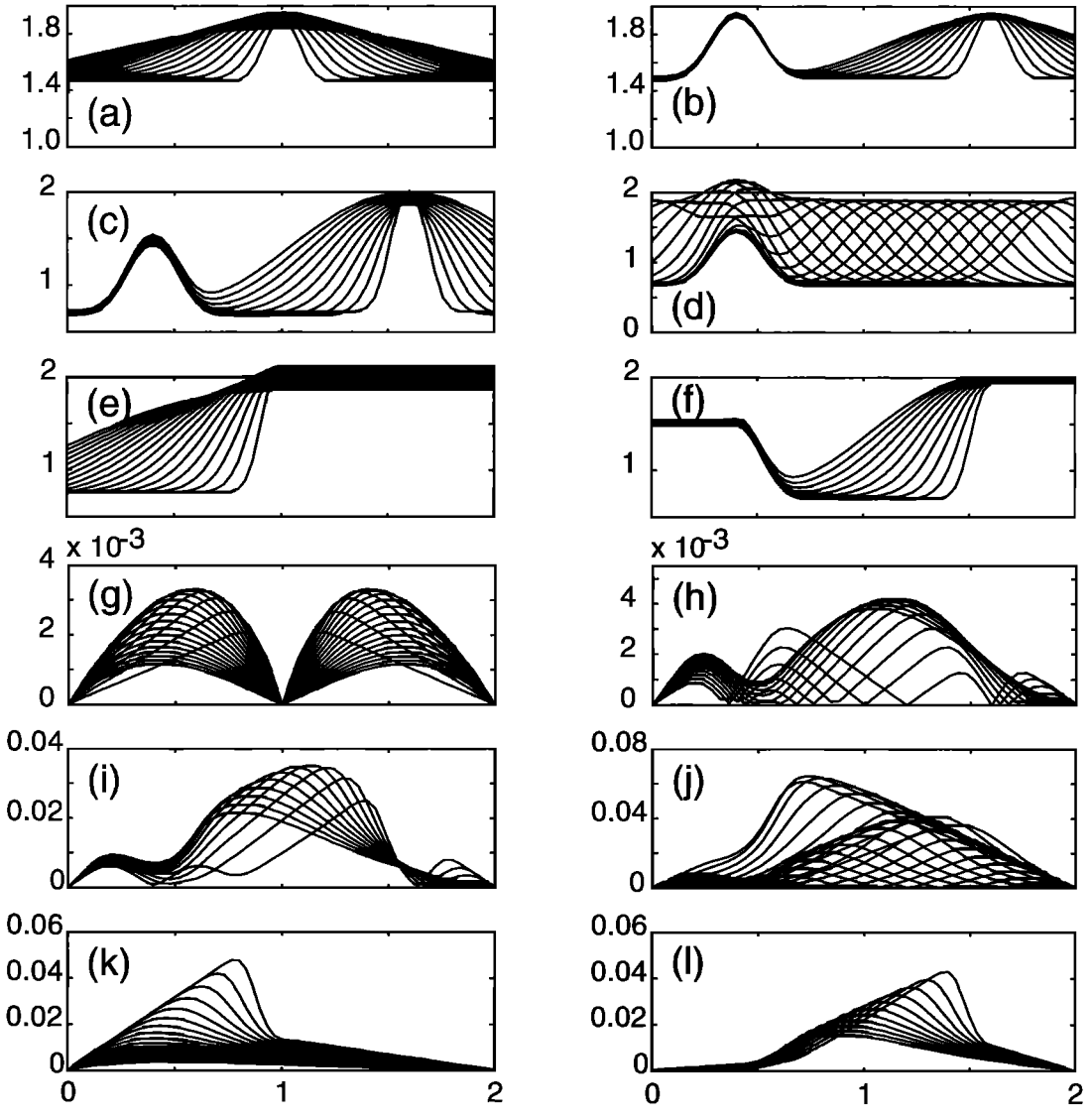

Figure 6. The amplitude of velocity (m/s) at the open end of the model as a function of the transverse distance (km) for all depth functions: each curve shows the result calculated from one depth function. (a–f) The amplitude of longitudinal velocity. (g–l) The amplitude of the transverse velocity. Figures 6a–6f (or Figures 6g–6l) correspond to the depth functions defined in Figures 1a–1f, respectively.

portant in the along-channel momentum balance as the width becomes comparable to the deformation radius. For these reasons, the present model is appropriate only for narrow estuaries.

4. Discussion

We have presented a solution of a 2-D tidal model for a narrow estuary with arbitrary lateral depth variation, and we have applied it to various depth profiles. Now we will further discuss the solution. We will compare model results to some observations obtained in the James River Estuary. We will fit the data to the phase of the longitudinal momentum equation to estimate the bottom drag coefficient, and we will apply the analytic model, using the estimated C_D and the real bathymetry, to where observations took place in the James River Estuary.

4.1. Comparison With Observations

Previous observations showed some bathymetric influences on tidal flow in shallow estuaries similar to those presented by the solution. For instance, the study of *Jay and Smith* [1990] indicated that the M_2 tidal current amplitude in the Columbia River Estuary is larger at the mouth and decreases toward the head. Acoustic Doppler current profiler (ADCP) observations in the lower Chesapeake Bay [*Valle-Levinson and Lwiza*, 1995, 1997] and the bay entrance [*Valle-Levinson et al.*, 1998] showed that the semidiurnal tidal velocity amplitude

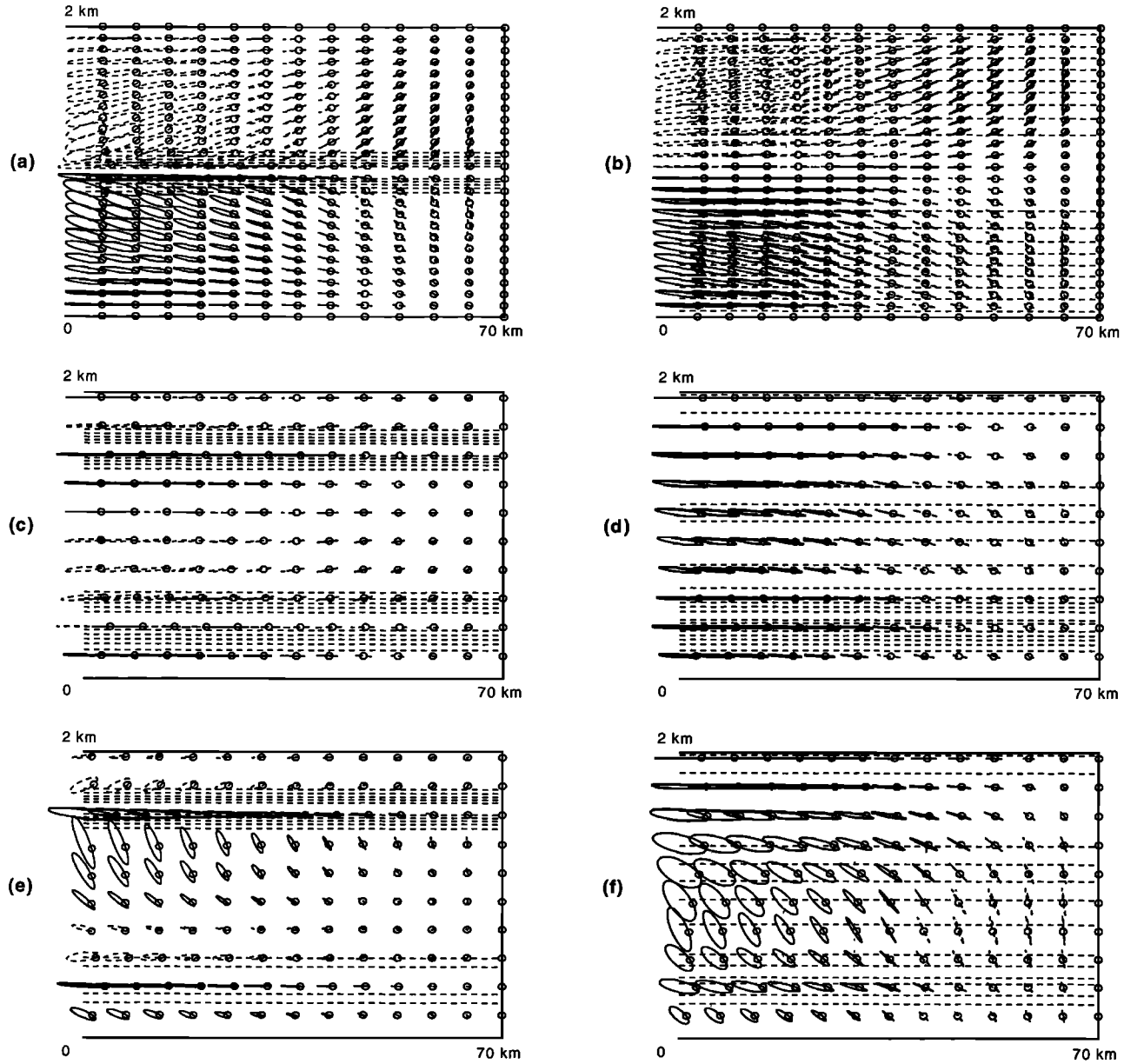

Figure 7. Tidal ellipses with the depth functions defined in equations (21)–(23). The circles indicate the position of the velocity vector at high tide (when the elevation is at its maximum value). The solid ellipses represent counterclockwise rotation, and the dashed ellipses represent clockwise rotation of the velocity vector. The depth contours are shown by dashed straight lines. (a) The depth function is equation (21) and $b = 100$ m. (b) $b = 1000$ m. (c) The same as Figure 7a except that the depth function in equation (22) is used. (d) The same as Figure 7c except that $b = 600$ m. (e) The same as Figures 7a and 7c except that equation (23) is used as the depth function. (f) The same as Figure 7e except that $b = 600$ m.

was higher in the navigational channels (0.5–0.6 ms^{-1}) and weaker (0.3 ms^{-1}) over the shoals. The flow in the channels also exhibited lags in phase compared to the adjacent shoals by $\sim 30°$ or 1 hour. These results are consistent with the present analytic model. Next, we will show more observational evidence in the James River Estuary.

Velocity profiles were sampled along two cross-estuary, 4- km long transects in the lower James River (Figure 11a) throughout two spring (October 26–27) and two neap tidal cycles (November 2–3) in 1996. The profiles were obtained during 25-hour cruises with a 600 kHz broadband RD Instruments' ADCP. The ADCP was mounted looking downward on a small (roughly 1.2 m long) catamaran and towed at 2.5 ms^{-1} to the side of a small boat. The ADCP recorded profiles of velocities which were averaged over 30 s intervals and gave a horizontal spatial resolution of $\sim$ 75 m. The vertical

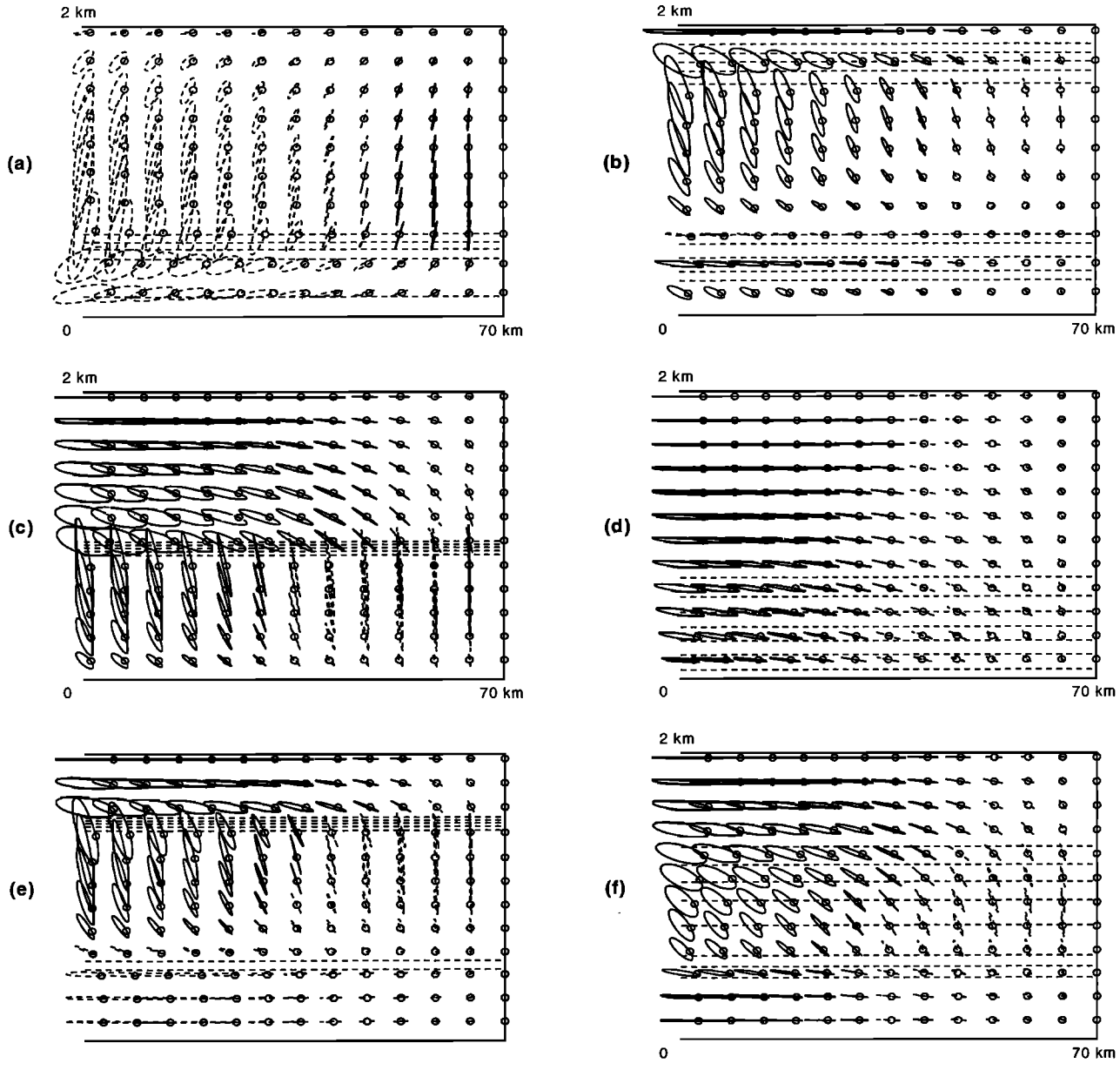

Figure 8. Tidal ellipses. (a) The same as Figure 7 except that here the depth function is equation (24) and $y_0 = 0$. (b) The same as Figure 8a except that $y_0 = 0.95D$. (c) The same as Figure 7a except that equation (25) is used for the depth function. (d) The same as Figure 8c except that $b = 1000$ m. (e) The same as Figure 8c except that equation (26) is used for the depth function. (f) The same as Figure 8e except that $b = 600$ m.

resolution was 0.5 m, and the closest bin to the surface was located at $\sim$ 2 m below the surface. Compass calibration and data correction were performed following *Joyce* [1989]. Navigation was carried out with differential Global Positioning System (GPS). In addition to the underway sampling, which provided spatial coverage, moored digiquartz pressure sensors (SeaBird SBE 26) were deployed at both ends of one transect and validated the assumption of small cross-estuary variations of surface elevation ($\sim$ 5%) relative to the tidal amplitude (Figure 11b). The time series of current velocity recorded at each point along each transect and at each depth consisted of 20 values for the spring tide cruise and 17 values for the neap tide cruise. These time series spanned two tidal cycles and were subject to least- squares harmonic analysis on the semidiurnal and diurnal frequencies [e.g., *Valle-Levinson et al.*, 1998]. The analysis yielded the across-estuary distribution of the semidiurnal tidal current amplitude shown in Figure 12. The along-estuary tidal current amplitude was clearly influenced by bathymetry as explained by the analytic solution. Greatest values were found in the channel, and weakest values were seen over the shoals. The small channel to the southwest of transect 1, por-

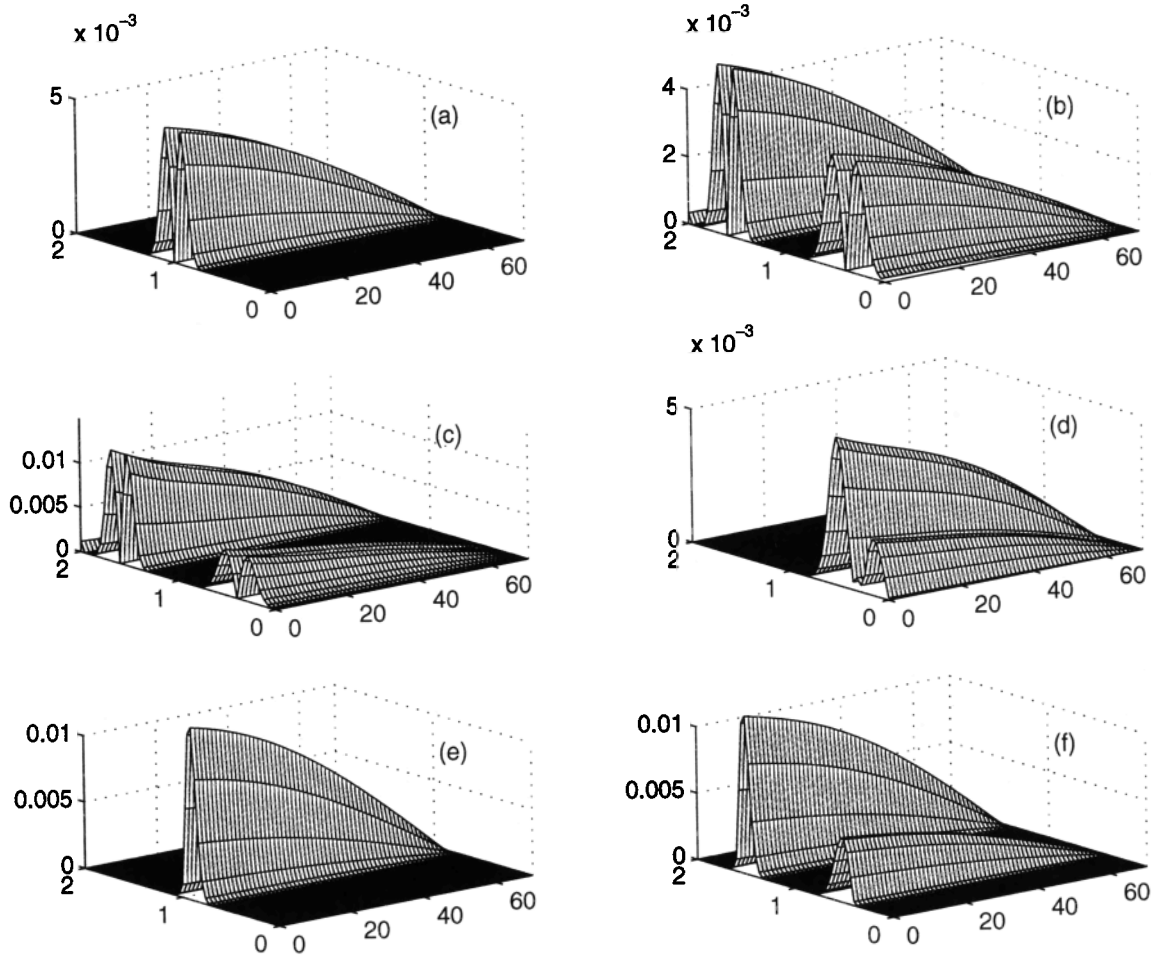

Figure 9. Amplitude of the vorticity (s^{-1}). (a–f) Amplitudes corresponding to the depth functions defined by (21)–(26), respectively, with the smallest parameter values (which generate the largest slopes).

traying bathymetry similar to that of Figure 1c, showed a local maximum in tidal current amplitude, similar to the analytic solution presented in Figures 2–3.

To quantitatively compare the model results with the observations, we now use the actual bathymetry (depth function across the two transects) and apply the analytic model to both transects at spring and neap tides. For simplicity, we assume a constant drag coefficient, which can be estimated from the phase relation of (8). By virtue of (8), we have the phase relationship

$$\phi_U = \phi_B + \phi_{Ax} \tag{27}$$

in which ϕ_U, ϕ_B, and ϕ_{Ax} are the phase values for U, $-g/(i\sigma + \beta/h)$, and $\partial A/\partial x$, respectively. Since we are interested in narrow estuaries in which the length scale of the depth variation is much smaller than the length scale of the phase variation of the along-channel pressure gradient across the channel, ϕ_{Ax} can be considered as a constant along a transect. The value for ϕ_B is

$$\phi_B = -\tan^{-1}\left(\frac{\sigma h}{\beta}\right) \tag{28}$$

Taking ϕ_{Ax} and β as two unknowns, we may find their values by fitting (27) to the observed phase of the depth-averaged tidal velocity using a least- squares method. We then use the obtained β to calculate the drag coefficient from (2). This method is more dynamically oriented than a simple scaling [*Godfrey*, 1980] and simpler than the adjoint numerical method [e.g., *Ullman and Wilson*, 1998]. The drag coefficients obtained by this approach are 1.5×10^{-3} and 1.8×10^{-3} for the spring and neap tides, respectively. The drag coefficients are then used with the analytic model. It should be noted that *Wang and Craig* [1993] also used a fitting technique to estimate parameters of friction, but they used the solution of a simplified model and were thus limited to the specific solution. In contrast, here we only use the momentum balance. Therefore the method presented here is not limited to the simple geometry and depth functions we have chosen. The comparison between the model-produced tidal amplitude and phase and those of the observations is shown in Figures 13–15. The model has reproduced the observed features of tidal amplitude and phase as functions of the water

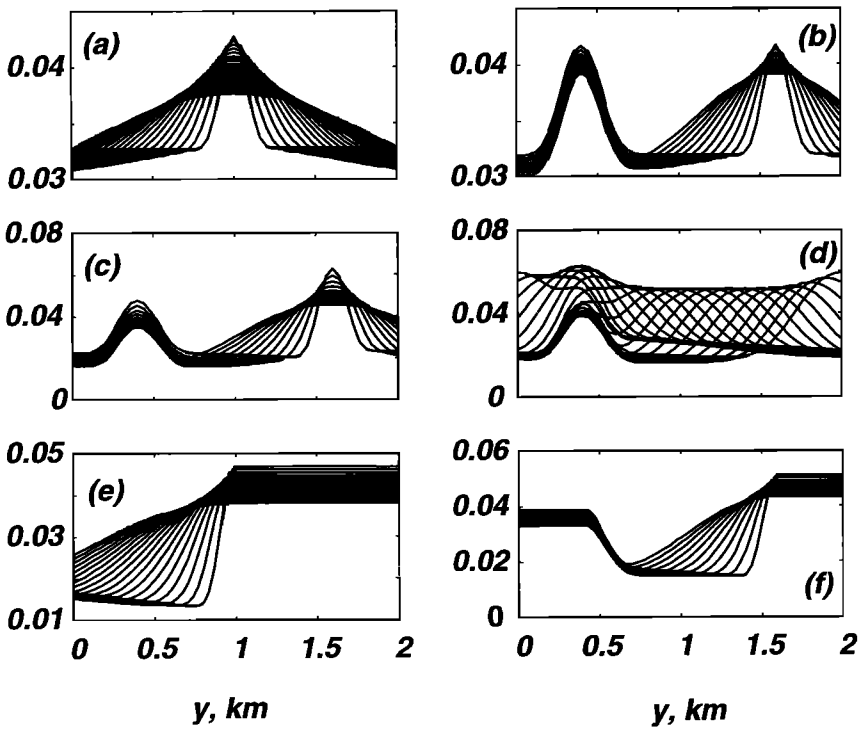

Figure 10. Maximum relative error of the model (percent), $|(\partial\zeta/\partial y)/(a/D)|$, which is proportional to the transverse gradient of surface elevation. (a–f) Maximum relative errors corresponding to the depth functions defined by (21)–(26), respectively. The maximum relative error is of the order of 5%.

depth. Particularly, the observed increase of amplitude of the along-channel velocity with the increase of water depth is similar to that shown by the model (Figure 13). The rate of increase decreases as depth increases, as mentioned at the end of section 2. The observed transverse phase difference of the along-channel velocity had the same order of magnitude as that predicted by the model (Figure 14): about 30°–40°, or roughly 1 hour in time. The phase of along-channel velocity at shallow water leads that at deep water. The amplitude of the transverse velocity from the observation appeared to be larger than the model result (Figure 15a). The observed phase (20°) of the transverse velocity is larger than the model result (15°) but otherwise with the same trend (Figure 15b). The quantitative agreement demonstrates that the model, although simple in dynamics, represented the main tidal properties well. We also note that there are apparent discrepancies between the model and observations, particularly in the amplitude of the transverse velocity. This could be caused by the oversimplification of the model. For example, here we are using a constant drag coefficient. In reality, the drag coefficient can be a function of position. In addition, stratification, meandering of the channel, along-estuary variation of the bathymetry, and advection of momentum are neglected in our model. The errors of the momentum and continuity equations are again due to the approximation taking ζ as independent of y. The estimated maximum relative error for the simplified James River Estuary model, as defined by the magnitude of $(\partial\zeta/\partial y)/(\zeta/D)$ is $\sim$ 2.5%. This value is smaller than the observed value of $\sim$ 5% (Figure 11b), a fact that may be related to all sources of errors not included in the model.

4.2. Significance of This Work

This work presents a series of steps and approximations that allow the depth-averaged tidal velocity to be resolved in a two-dimensional domain. The solution is obtained from a complete set of dynamic equations for a tidal wave and does not need to specify the pressure gradient as in the work of *Friedrichs and Hamrick* [1996]. In addition, the solution for the transverse velocity is obtained by integration of the continuity equation, which makes the results insensitive to the form of the transverse momentum balance. The method allows an arbitrary lateral depth variation in a two-dimensional model. As a result, this solution provides a convenient way to study the effects of arbitrary lateral depth variation on the tidal current. Variable depth functions usually make the problem too complicated to allow an analytic solution to be obtained in a simple way. For an arbitrary depth function, it often becomes even more remote to permit an analytic solution without a simplification. In a numerical model, a strong bottom slope such as those represented by the functions used here (Figures 1a–1f) may cause convergence problems. This analytic solution can also be useful for testing of numerical models [e.g., *Thacker*, 1981; *Lynch and Gray*, 1978; *Chen*, 1989]. Since the present solution allows ar-

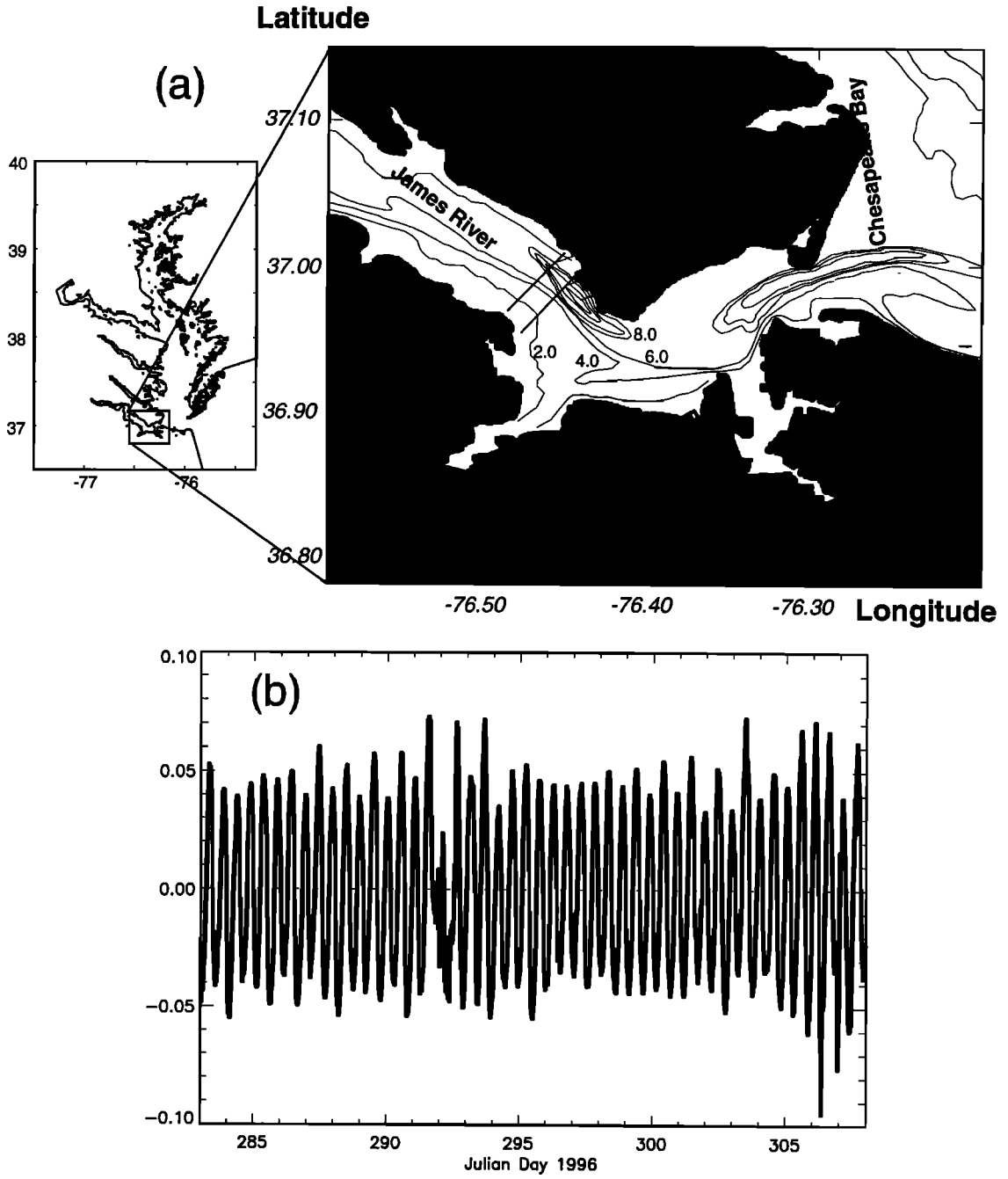

Figure 11. (a) Area of study showing sampling transects. (b) Time series of transverse variation of surface elevation (percentage of the elevation) obtained from two pressure sensors across the James River in 2 months. For better visualization, only one month data representative of the whole record are shown.

bitrary depth functions, it may be particularly valuable for testing of high-order numerical models with large depth gradients.

5. Summary

We have presented a solution for a two-dimensional depth-averaged model of tidal motion in narrow estuaries with arbitrary lateral depth variations. The solution is obtained by assuming that the lateral variation of the surface elevation is small in narrow estuaries. The lateral variation of elevation calculated from this solution is indeed small (~ 5% of the tidal amplitude). The model is in contrast to that of *Friedrichs and Hamrick* [1996] in which the along-channel pressure gradient was prescribed, rather than being part of the solution. This model resolves the tidal wave propagation and velocity field in a two-dimensional domain, rather than along a single section [*Friedrichs and Hamrick*, 1996]. Combined with the along-channel momentum equation, a cross-channel integration of the continuity highly simplifies the mathematics for the tidal elevation and, at

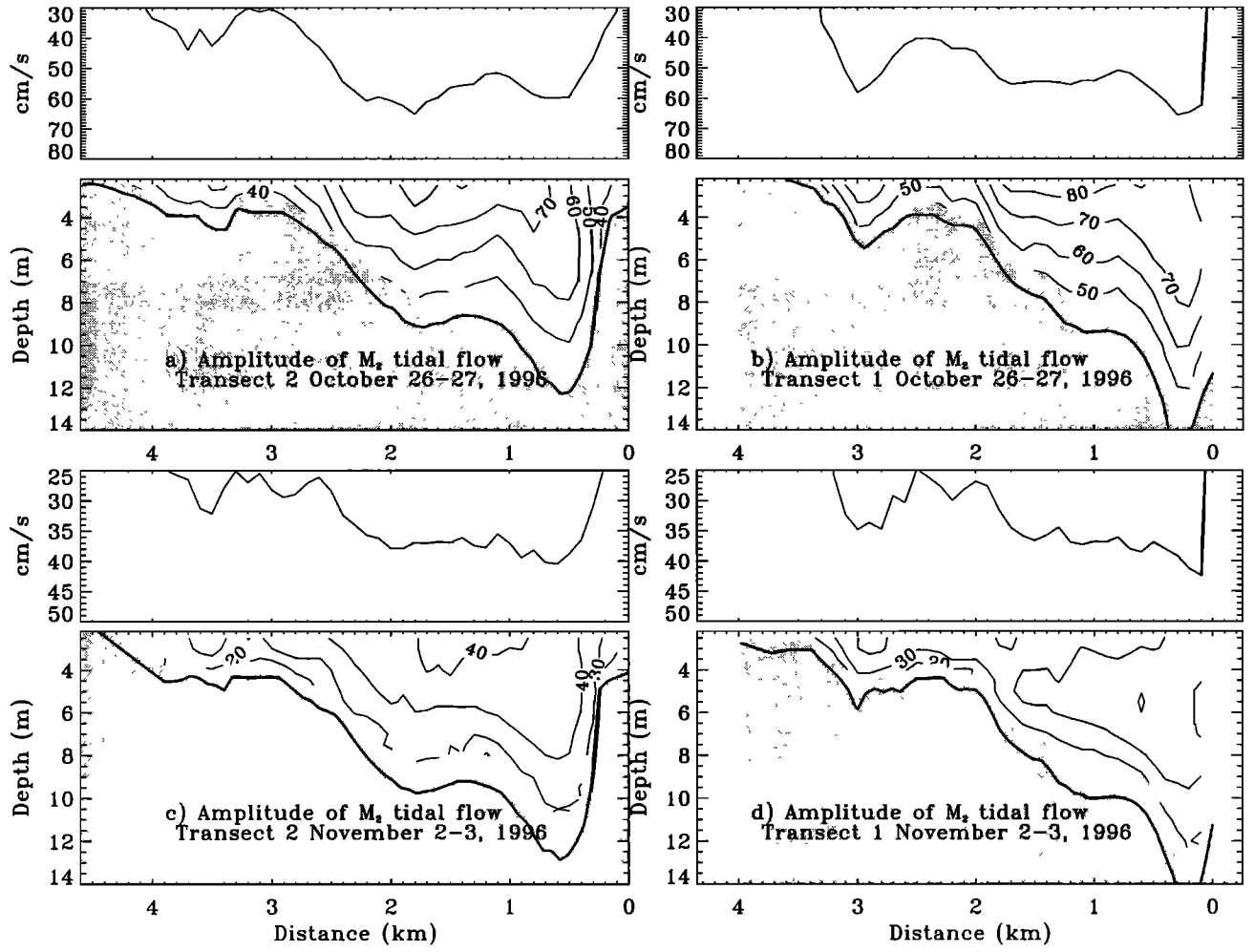

Figure 12. M_2 tidal current amplitude (cm/s) and the corresponding depth-averaged values obtained from observations at two transects in the James River Estuary during two cruises in October - November, 1996. (a) Amplitude along transect 2, October 26-27, 1996. (b) Amplitude along transect 2, November 2-3, 1996. (c) Amplitude along transect 1, October 26-27, 1996. (d) Amplitude along transect 1, November 2-3, 1996.

the same time, allows an arbitrary depth function. The solution is compact and easy to apply to different depth functions.

It should be emphasized that the tidal elevation is solved without using the transverse momentum equation. The transverse velocity is obtained from continuity. The transverse momentum equation is only used to check the validity of the uniformity assumption for the elevation. As a result, only $\partial A/\partial y$ is crucially sensitive to the precise form of the cross-channel balance. This approach makes the solution not sensitive to the transverse momentum balance.

Dozens of depth functions in six groups with various degrees of bottom slopes are applied to calculate the solution. The velocity field is highly correlated with the depth variations. The longitudinal velocity is stronger at the mouth than it is in the interior and stronger in deep waters than it is over the shoals. The transverse velocity has weak longitudinal variability and is small in the channels and on the sides but is relatively large on the edges of the maximum bottom slopes. The tidal ellipses are also sensitive to the depth variation. At the mouth, the flow behaves as a progressive or partially progressive wave and at the head as a standing wave. The vorticity of the flow is greatest where depth changes most dramatically and can reach 10^{-3} and even 10^{-2} s^{-1} over very large depth slopes. This shear flow should therefore contribute to increase the dispersion coefficient, a subject that we have omitted for the moment. It is found that with a maximum relative error of 5%, the solution satisfies both momentum and mass balances.

ADCP observations along two transects of $\sim$ 4 km in the James River Estuary during two cruises in 1996 showed characteristics similar to those of the analytic solution. By fitting the observed phase of the semidiurnal tide to the phase relationship of the longitudinal momentum equation, we estimated the bottom drag co-

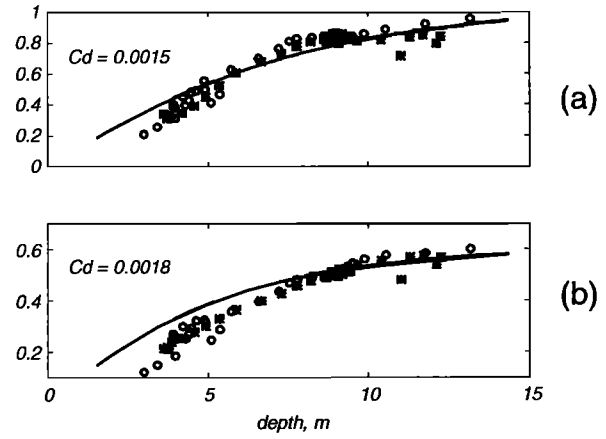

Figure 13. Amplitude of the along-channel semidiurnal tidal velocity (m/s) as a function of depth. The solid curves are from the model. The circles and stars are from observations at the first and second transects, respectively. (a) Spring tides. (b) Neap tides.

efficient to be 1.5 $\times 10^{-3}$ and 1.8 $\times$ 10^{-3} for the spring and neap tides, respectively. This method of drag coefficient estimation is much simpler than the traditional adjoint numerical modeling technique. Using these values of drag coefficient and the real bathymetry along the two transects in the James River Estuary, we calculated the analytical solution which showed remarkable agreement with observations. The relative error (or the ratio between the transverse difference of elevation and the elevation) of the simplified James River Estuary model is about 2.5%. Two months of time series data from pressure sensors at two sides of the James River Estuary showed small transverse difference of elevation ($\sim$ 5%). The slightly higher-than-theory value of the transverse difference in elevation could be caused by the curvature of the coastlines and other factors which are not included in the present model.

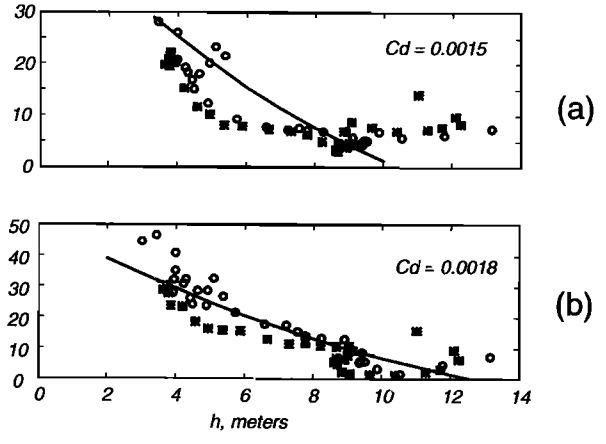

Figure 14. Phase (in degrees) of the along-channel semidiurnal tidal velocity as a function of depth. The solid curves are from the model. The circles and stars are from observations at the first and second transects, respectively. (a) Spring tides. (b) Neap tides.

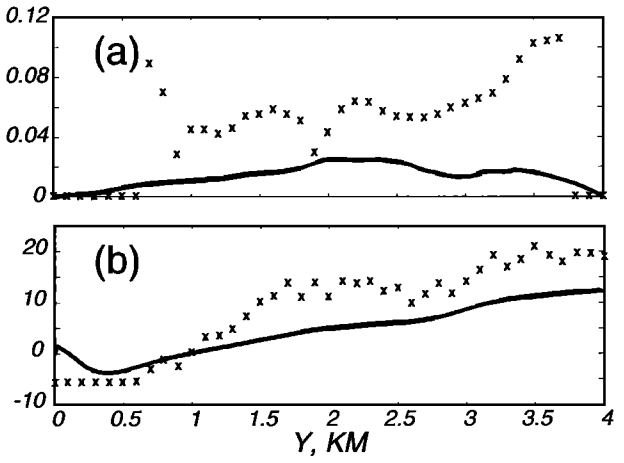

Figure 15. (a) Amplitude of the transverse semidiurnal tidal velocity (m/s) as a function of depth. (b) Phase (in degrees) of the transverse semidiurnal tidal velocity as a function of depth. The solid curves are from the model. The stars are from observations at the first transect.

Appendix: The Solution Expressed in Detail

In this appendix, we will express the solution in detail so that the real and imaginary parts are separated. It should be noted, however, that with some software (e.g., MATLAB) the solution in its complex form can be calculated directly without separating the real and imaginary parts. Nevertheless, this appendix is presented here for completeness. It can be shown, by a straightforward mathematical derivation, that the complex form of the solution for A can be expressed as

$$A = a\frac{\lambda_0}{L}\left(\tau_1{}^2+\tau_2{}^2\right)^{1/4}\left[a_1\cos(\frac{\phi}{2})-a_2\sin(\frac{\phi}{2})+i\left(a_1\sin(\frac{\phi}{2})+a_2\cos(\frac{\phi}{2})\right)\right] \tag{A1}$$

in which i, $\lambda_0 = \sqrt{gh_0}/\sigma$, L, and a are $\sqrt{-1}$, the frictionless wavelength, the length of the estuary, and the tidal amplitude at the mouth, respectively, and

$$\begin{aligned}
&\tau_1 = -\tau_0\int_0^1\frac{dy'}{1+\tau^2}, \quad \tau_2 = \int_0^1\frac{\tilde{h}dy'}{1+\tau^2}\\
&\tau_0 = \frac{\beta}{\sigma h_0}, \quad \tau = \frac{\beta}{\sigma h}\\
&\tilde{h} = \frac{h}{h_0}, \quad y' = \frac{y}{D}\\
&\omega_1 = \frac{1}{\lambda_0}(\tau_1^2+\tau_2^2)^{-1/4}\cos(\frac{\phi}{2})\\
&\omega_2 = \frac{1}{\lambda_0}(\tau_1^2+\tau_2^2)^{-1/4}\sin(\frac{\phi}{2})\\
&\phi = \tan^{-1}\left(\frac{\tau_1}{\tau_2}\right)\\
&a_1 = \cos\left[\omega_1(x-L)\right]\cosh\left[\omega_2(x-L)\right]\\
&a_2 = \sin\left[\omega_1(x-L)\right]\sinh\left[\omega_2(x-L)\right]
\end{aligned} \tag{A2}$$

where β, h_0, h, σ, and D are the linear friction coefficient, the transverse mean depth, the depth function, the angular tidal frequency, and the width of the estuary, respectively. A dimensionless version of (A1) can be obtained by dividing by a. In (A1), there are two parameters: (1) the ratio between the frictionless wavelength scale λ_0 and the length of the model L and (2) the ratio between the tidal time-scale σ^{-1} and the frictional decay time-scale h_0/β, i.e., τ_0. In addition, there is also a function τ, similar to τ_0. The difference of τ is that $h(y)$ instead of h_0 is used. The terms or factors in (A1) are determined with either of these two ratios or with a transverse integration of a function of τ. The along-channel decay of the tidal amplitude due to friction is represented by a_1 and a_2.

The longitudinal gradient of A can be expressed as

$$\frac{dA}{dx} = \frac{a}{\lambda_0}\left(\tau_1^2+\tau_2^2\right)^{-1/4}\frac{1}{b_1^2+b_2^2}(\tilde{A}_1+i\tilde{A}_2) \tag{A3}$$

where

$$\begin{aligned}\tilde{A}_1 = \; & b_1\left[c_1\cos(\frac{\phi}{2})-c_2\sin(\frac{\phi}{2})\right] \\ & -b_2\left[c_2\cos(\frac{\phi}{2})+c_2\sin(\frac{\phi}{2})\right]\end{aligned} \tag{A4}$$

$$\begin{aligned}\tilde{A}_2 = \; & b_1\left[c_1\cos(\frac{\phi}{2})+c_2\sin(\frac{\phi}{2})\right] \\ & +b_2\left[c_2\cos(\frac{\phi}{2})-c_2\sin(\frac{\phi}{2})\right]\end{aligned} \tag{A5}$$

$$\begin{aligned}&b_1=\cos(\omega_1 L)\cosh(\omega_2 L), \quad b_2=\sin(\omega_1 L)\sinh(\omega_2 L)\\ &c_1=\sin\left[\omega_1(x-L)\right]\cosh\left[\omega_2(x-L)\right]\\ &c_2=\cos\left[\omega_1(x-L)\right]\sinh\left[\omega_2(x-L)\right]\end{aligned} \tag{A6}$$

It can be seen that dA/dx is of the order of a/λ_0, an expected result.

Similarly, the complex amplitude of the longitudinal velocity can be expressed as

$$\begin{aligned}U \; = & -\frac{a}{h_0}\sqrt{gh_0}\frac{\left(\tau_1{}^2+\tau_2{}^2\right)^{-1/4}}{(b_1^2+b_2^2)(1+\frac{\beta^2}{h^2\sigma^2})} \\ & \left[\tilde{A}_1+\frac{\beta}{h\sigma}\tilde{A}_2+i\left(\tilde{A}_2-\frac{\beta}{h\sigma}\tilde{A}_1\right)\right]\end{aligned} \tag{A7}$$

in which $(a/h_0)\sqrt{gh_0}$ is the frictionless velocity scale, the factors $(\tau_1{}^2+\tau_2{}^2)^{-1/4}$ and $1/(b_1^2+b_2^2)$ show the effect of friction, and the factor $1/(1+\beta^2/(h^2\sigma^2))$ shows the variability of friction contributed by the variation of depth.

Acknowledgments.

This work was supported by the U.S. National Science Foundation (NSF Project OCE-9529806) and by the Center for Coastal Physical Oceanography (CCPO), Department of Oceanography, Old Dominion University (ODU). Dozens of faculty members, staff, and students from ODU, State University of New York, and University of Delaware participated in the field work, and their help was invaluable. The assistance on the field of R. Bray, R.C. Kidd, and W. Check is greatly appreciated. We would like to thank J. H. Simpson for providing us with information of some previous work. C. Friedrichs' review comments are also highly appreciated. Additional data related to the James River may be found at the following homepage: http://www.ccpo.odu.edu/~arnoldo/transcope/transcope.html.

References

Carrier, G. F., Gravity waves on water of variable depth, *J. Fluid Mech.*, *24*, 641-659, 1966.

Chen, C. L., Analytic solutions for tidal model testing, *J. Hydraul. Eng.*, *115*, 1707-1714, 1989.

Defant, A., *Physical Oceanography*, 598 pp., vol. 2, Pergamon, Tarrytown, N.Y., 1961.

Friedrichs, C.T., and J. M. Hamrick, Effects of channel geometry on cross sectional variations in along channel velocity in partially stratified estuaries, in *Buoyancy Effects on Coastal and Estuarine Dynamics, Coastal Estuarine Stud.*, vol. 53, edited by D.G. Aubrey and C.T. Friedrichs, pp. 283-300, AGU, Washington, D.C., 1996.

Godfrey, J. S., A numerical model of James River Estuary, Virginia, U.S.A., *Estuarine Coastal Mar. Sci.*, *11*, 295-310, 1980.

Ippen, T., and D. R. F. Harleman, One-dimensional analysis of salinity intrusion in estuaries, *Tech. Bull. 5*, U.S. Army Corps of Eng., Vicksburg, Miss., 1961.

Jay, D., and D. Smith, Circulation, density distribution and neap-spring transitions in the Columbia River Estuary, *Prog. Oceanogr.*, *25*, 81-112, 1990.

Joyce, T. M., On in situ "calibration" of shipboard ADCPs, *J. Atmos. and Oceanic Technol.*, *6*, 169-172, 1989.

Keller, J. B., Surface waves on water of non-uniform depth, *J. Fluid Mech.*, *4*, 607-614, 1958.

Lamb, H., *Hydrodynamics*, Cambridge Univ. Press, 738 pp., New York, 1932.

LeBlond, P. H., On tidal propagation in shallow rivers, *J. Geophys. Res.*, *83*, 4717-4721, 1978.

Li, C., Tidally induced residual circulation in estuaries with cross channel bathymetry, Ph.D. dissertation, 242 pp., Univ. of Conn., Storrs, 1996.

Li, C., and J. O'Donnell, Tidally driven residual circulation in shallow estuaries with lateral depth variation, *J. Geophys. Res.*, *102*, 27,915-27,929, 1997.

Lynch, D. R., and W. G. Gray, Analytic solutions for computer flow model testing, *J. Hydraul. Div., Am. Soc. Civ. Eng.*, *104*, 14105-1428, 1978.

Nachbin, A., and G. C. Papanicolaou, Water waves in shallow channels of rapidly varying depth, *J. Fluid Mech.*, *241*, 311-332, 1992.

Officer, C. B., *Physical Oceanography of Estuaries*, John Wiley, New York, 1976.

Oliveira, A., and A. M. Baptista, *Computational Methods in Water Resources XI*, vol. 2, *Computational Methods in Surface Flow and Transport Problems*, pp. 355-362, Computational Mechanics, Southampton, England, 1996.

Parker, B. B., Frictional effects on the tidal dynamics of shallow estuary, Ph.D. dissertation, 291 pp., Univ. of Johns Hopkins, Baltimore, Md., 1984.

Parker, B. B., The relative importance of the various nonlinear mechanisms in a wide range of tidal interactions (review), in *Tidal Hydrodynamics*, edited by B. B. Parker, pp. 237-268, John Wiley, New York, 1991.

Prandle, D., Classification of tidal response in estuaries from channel geometry, *Geophys. J. R. Astron. Soc.*, *80*, 209-221, 1985.

Proudman, J., *Dynamical Oceanography*, 409 pp., New York, Methuen, 1953.

Speer, P. E., and D. G. Aubrey, A study of nonlinear tidal propagation in shallow inlet/estuarine systems, II, Theory, *Estuarine, Coastal Shelf Sci., 21*, 207-222, 1985.

Taylor, G. I., Tidal oscillations in gulfs and rectangular basins, *Proc. London Math. Soc., Ser. 2, 20*, 148-181, 1921.

Thacker, W. C., Some exact solutions to the nonlinear shallow-water wave equations, *J. Fluid Mech., 107*, 499-508, 1981.

Ullman, D. S., and R. E. Wilson, Model parameter estimation from data assimilation modeling: Temporal and spatial variability of bottom drag coefficient, *J. Geophys. Res., 103*, 5531-5549, 1998.

Valle-Levinson, A., C. Li, T. Royer, and L. P. Atkinson, Flow regimes in lower Chesapeake Bay, *Cont. Shelf Res., 18*, 1157-1177, 1998.

Valle-Levinson, A., and K. M. M. Lwiza, The effects of channels and shoals on exchange between the Chesapeake Bay and the adjacent ocean, *J. Geophys. Res., 100*, 18,551-18,563, 1995.

Valle-Levinson, A., and K. M. M. Lwiza, Bathymetric influences on the lower Chesapeake Bay hydrography, *J. Mar. Syst., 12*, 221-236, 1997.

Wang, X. H., and P. D. Craig, An analytic model of tidal circulation in a narrow estuary, *J. Mar. Res., 51*, 447-465, 1993.

C. Li and A. Valle-Levinson, Center for Coastal Physical Oceanography, Crittenton Hall, Old Dominion University, Norfolk, VA 23529. (e-mail: chunyan@ccpo.odu.edu)

(Received April 22, 1998; revised April 5, 1999; accepted May 3, 1999.)